J Mater Sci: Mater Med (2008) 19:3063–3070
DOI 10.1007/s10856-008-3442-1

Preparation, characterization and mechanical performance of dense β-TCP ceramics with/without magnesium substitution

Xing Zhang · Fengchun Jiang · Todd Groth · Kenneth S. Vecchio

Received: 29 November 2007 / Accepted: 19 March 2008 / Published online: 5 April 2008

Abstract Beta-tricalcium phosphate (β-TCP) powder was prepared by a two-step process: wet precipitation of apatitic tricalcium phosphate [$Ca_9(HPO_4)(PO_4)_5(OH)$] (β-TCP 'precursor') and calcination of the precursor at 800°C for 3 h to produce β-TCP. Magnesium-substituted tricalcium phosphate (β-TCMP) was produced by adding $Mg(NO_3)_2 \cdot 6H_2O$ into $Ca(NO_3)_2$ solution as Mg^{2+} source before the precipitation step. The transition temperature from β-TCP to α-TCP increases with the increase of Mg^{2+} content in β-TCMP. β-TCMP with 3 mol.% Mg^{2+} has β-TCP to α-TCP transition temperature above 1,300°C. Dense β-TCMP (3 mol.% Mg^{2+}) ceramics (~99.4% relative density) were produced by pressing the green bodies at 100 MPa and further sintering at 1,250°C for 2 h. The average compressive strength of dense β-TCP ceramics sintered at 1,100°C is ~540 MPa, while that of β-TCMP (3 mol.% Mg^{2+}) ceramics is ~430 MPa.

1 Introduction

Tricalcium phosphate [$Ca_3(PO_4)_2$, TCP] ceramics, especially β-TCP, are currently used for a number of dental and skeletal prosthetic applications due to their good biocompatibility and osteointegration properties [1–6]. TCP can exist under three polymorphs [7, 8]: (i) β-TCP is stable below 1,120°C, with space group $R\bar{3}c$ and a room temperature density of 3.07 g cm^{-3}. (ii) α-TCP is stable from 1,120 to 1,470°C, but can be quenched to room temperature as a metastable phase, with space group $P2_1/a$ and a room temperature density of 2.86 g cm^{-3}. (iii) α′-TCP is stable from 1,470°C to the melting point at 1,756°C. Recently, Yashima and Sakai [9] reported that the space group of α′-TCP is $P\bar{3}m$.

Highly dense β-TCP ceramics are difficult to prepare, due to insufficient compaction when sintering below the β-TCP to α-TCP transition temperature [7, 10]. Above the transition temperature, β-TCP to α-TCP transformation causes the expansion of the material during the sintering process and creates micro-cracks in the ceramics, which prevents TCP ceramics from further densification [11, 12].

In this investigation, β-TCP powders with and without Mg substitution were produced. With the increase of Mg^{2+} content in β-TCMP [$(Ca,Mg)_3(PO_4)_2$], the β-TCP to α-TCP transition temperature increases [7, 13–15]; β-TCMP with 3 mol.% Mg^{2+} has its transition temperature above 1,300°C. In this study, dense β-TCP and β-TCMP ceramics were produced by cold pressing ceramic green bodies from the powders at 100 MPa, and subsequently pressureless sintering the green bodies above 1,150°C. Quasi-static compression tests of dense β-TCP and β-TCMP ceramics were performed to evaluate the mechanical strength of these ceramics. Due to the presence of Mg in calcified living tissues (about 0.5% in bone or tooth enamel and more than 1% in tooth dentine [16]), β-TCMP prepared in this investigation, may have improved biological functions [17–19], and potential applications in bone and tooth replacement and augmentation.

X. Zhang
Materials Science and Engineering Program, UC San Diego, La Jolla, USA

F. Jiang · T. Groth · K. S. Vecchio (✉)
Department of NanoEngineering, UC San Diego, La Jolla, USA
e-mail: kvecchio@ucsd.edu

2 Experimental

2.1 Synthesis of β-TCP and β-TCMP powders

Calcium nitrate tetrahydrate [$Ca(NO_3)_2 \cdot 4H_2O$, ACS reagent, Sigma-Aldrich], magnesium nitrate hexahydrate [$Mg(NO_3)_2 \cdot 6H_2O$, ACS reagent, Sigma-Aldrich] and ammonium phosphate dibasic [$(NH_4)_2HPO_4$, reagent grade, Sigma-Aldrich] were used as starting reagents, for calcium, magnesium and phosphorus, respectively.

Calcium nitrate solution was titrated to $(NH_4)_2HPO_4$ solution with continuous stirring (~700 rpm) and controlling final molar ratio of Ca/P as 1.5. $(NH_4)_2HPO_4$ solution was adjusted to pH ~10 before the titration and kept at pH ~9 during the titration with ammonium hydroxide solution. The precipitate (apatitic tricalcium phosphate) was rinsed with deionized water, separated by centrifuge and dried at 100°C for ~12 h. For β-TCMP, a predetermined amount of $Mg(NO_3)_2 \cdot 6H_2O$ as Mg^{2+} source was dissolved in the $Ca(NO_3)_2$ solution before the titration, and the final molar ratio of (Ca + Mg)/P is 1.5. The Mg content in the β-TCMP sample is calculated by the molar percentage of $Mg^{2+}/(Ca^{2+} + Mg^{2+})$ from the starting reagents. Hereafter, β-TCMP samples with 2 mol.%, 3 mol.%, 4 mol.%, 5 mol.%, and 10 mol.% Mg^{2+} in this investigation are designated as β-TCMP-2, β-TCMP-3, β-TCMP-4, β-TCMP-5 and β-TCMP-10, respectively. The dried precipitate (β-TCP or β-TCMP precursor) was calcined at 800°C in air for 3 h to produce β-TCP or β-TCMP.

2.2 Ceramic sintering

A specified amount of β-TCP or β-TCMP powder necessary to make a green body compact was ground with several drops of 5 wt.% polyvinyl alcohol (PVA) solution in a mortar. The powder mixture was uniaxially pressed in a stainless steel die on a load frame to 100 MPa pressure to create compacted green bodies. Green bodies were then pressureless sintered above 1,100°C in a muffle furnace in air, with a heating rate of 2°C/min and a dwell time of 2 h.

2.3 Characterization

Sample phases were identified by x-ray diffraction (XRD) using a Rigaku Rotaflex X-ray diffractometer, while the morphology of the structures was studied by scanning electron microscopy (SEM) using a Phillips XL20. Differential thermal analysis (DTA) and Thermogravimetric analysis (TGA) were employed to determine the phase stability and the reaction temperatures using a Pyris Diamond TG/DTA (PerkinElmer Instruments). Ceramic densities were determined by Archimedes' method using deionized water. Quasi-static compression tests were conducted on a servohydraulic load frame at a strain rate of 10^{-3}/s. For each ceramic, 10–15 cylindrical specimens [~11.0 mm (diameter) × 4.5 mm (height)] were tested.

3 Results and discussion

3.1 Powder characterization

Figure 1 shows an XRD pattern of the β-TCP precursor (apatitic tricalcium phosphate) as prepared at room temperature (Fig. 1a) and β-TCP after calcination of the precursor at 800°C for 3 h (Fig. 1b). Broad diffraction peaks in Fig. 1a indicate the β-TCP precursor has a small crystallite size and poor crystallinity. The diffraction peaks are close to those of hydroxyapatite (HAP, JCPDF #9-0432) as marked in the pattern, indicating the precursor has a similar structure as HAP. The precursor (apatitic tricalcium phosphate) is reported to have formula of $Ca_9(HPO_4)(PO_4)_5(OH)$ [20, 21].

After calcination of the precursor at 800°C for 3 h, good crystalline β-TCP formed (Fig. 1b). All peaks match with β-TCP (JCPDF #9-0169), with some indices labeled in the pattern.

The precipitation reaction and the calcination reaction to produce β-TCP are described by the reactions given in Eqs. 1 and 2 [21, 22], respectively.

$$9Ca(NO_3)_2 + 6(NH_4)_2HPO_4 + 6NH_4OH \rightarrow Ca_9(HPO_4)(PO_4)_5(OH) + 5H_2O + 18NH_4NO_3 \quad (1)$$

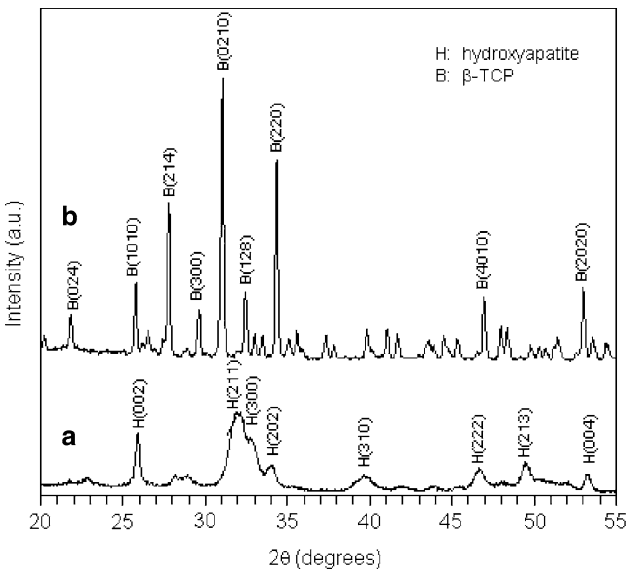

Fig. 1 XRD pattern of (**a**) β-TCP precursor (apatitic tricalcium phosphate) and (**b**) β-TCP after calcination of the precursor at 800°C for 3 h

$$Ca_9(HPO_4)(PO_4)_5(OH) \rightarrow 3Ca_3(PO_4)_2 + H_2O \quad (2)$$

The XRD patterns of β-TCMP-3 precursor as prepared (Fig. 2a) and β-TCMP-3 produced at 800°C (Fig. 2b) are similar to the corresponding pattern in Fig. 1, which indicates no new phase(s) formed during the precipitation and calcination process with the presence of Mg^{2+}. The diffraction peaks in Fig. 2b shift to larger angles, compared to those of β-TCP in Fig. 1b, consistent with the substitution of Ca^{2+} by Mg^{2+} in β-TCP structure.

The precipitation of β-TCMP precursor $[(Ca_{1-x}Mg_x)_9(HPO_4)(PO_4)_5(OH)]$ and its decomposition to β-TCMP $[(Ca_{1-x}Mg_x)_3(PO_4)_2]$ take place as Eqs. 3 and 4, respectively [23].

$$(9-9_x)Ca(NO_3)_2 + (9_x)Mg(NO_3)_2 + 6(NH_4)_2HPO_4 + 6NH_4OH \rightarrow (Ca_{1-x}Mg_x)_9(HPO_4)(PO_4)_5(OH) + 18NH_4NO_3 + 5H_2O \quad (3)$$

$$(Ca_{1-x}Mg_x)_9(HPO_4)(PO_4)_5(OH) \rightarrow 3(Ca_{1-x}Mg_x)_3(PO_4)_2 + H_2O \quad (4)$$

Figure 3 shows XRD patterns of β-TCMP samples with different Mg^{2+} content (up to 10 mol.%) produced at 800°C. All peaks in the pattern match with β-TCP, indicating the incorporation of Mg^{2+} into TCP structure. A maximum 14.3 mol.% Mg^{2+} can substitute for Ca^{2+} in the β-TCP structure without the formation of any new phases [13, 24]. With increasing Mg^{2+} content (Fig. 3a–d), the diffraction peaks shift to larger angles, indicating a contraction of the lattice constants. The refined lattice parameters (a and c) of β-TCP and β-TCMP were calculated from the diffraction patterns shown in Fig. 4. Six peaks [Miller indices (3 0 0), (0 2 10), (1 2 8), (3 0 6), (1 1 12) and (2 0 0)] in each diffraction pattern were refined to calculate 'a' and 'c' values. The lattice parameters in Fig. 4 are average values of lattice constants from at least 3 XRD patterns for each sample. Both 'a' and 'c' values decrease with increasing Mg^{2+} content (up to 10 mol.%), due to the smaller ionic radius of Mg^{2+} (0.65 Å) compared to Ca^{2+} (0.99 Å) [25].

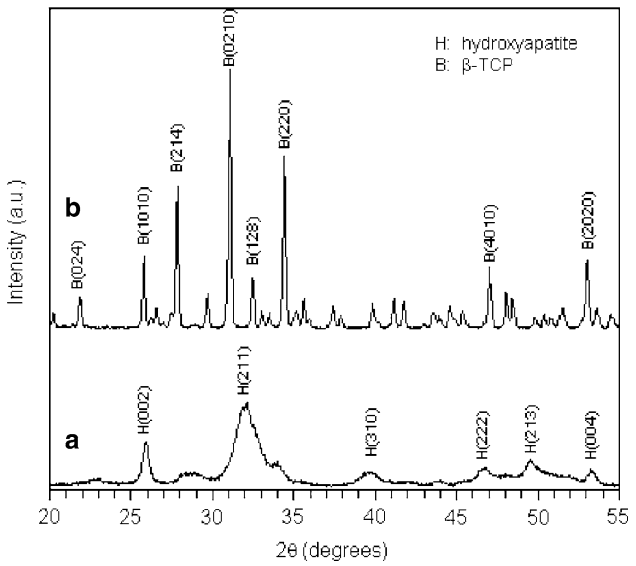

Fig. 2 XRD pattern of β-TCMP-3 (3 mol.% Mg^{2+}) precursor (**a**) and β-TCMP-3 after calcination (**b**) of precursor at 800°C for 3 h

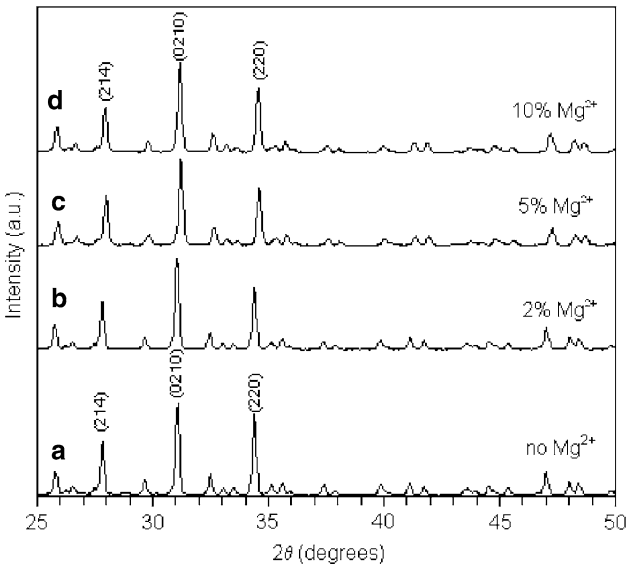

Fig. 3 XRD pattern of (**a**) β-TCP, (**b**) β-TCMP-2, (**c**) β-TCMP-5 and (**d**) β-TCMP-10, produced at 800°C

Figure 5a shows TG/DTA results of β-TCMP-3 precursor heated in air to 1,300°C with a heating rate of 5°C/min. The small endothermic peak around 725°C in the DTA curve indicates the decomposition of the precursor to form β-TCMP, according to the reaction described by Eq. 4. The weight loss that occurs at approximately the same temperature in the TG curve is the loss of water from the decomposition reaction. Figure 5b shows the DTA result of

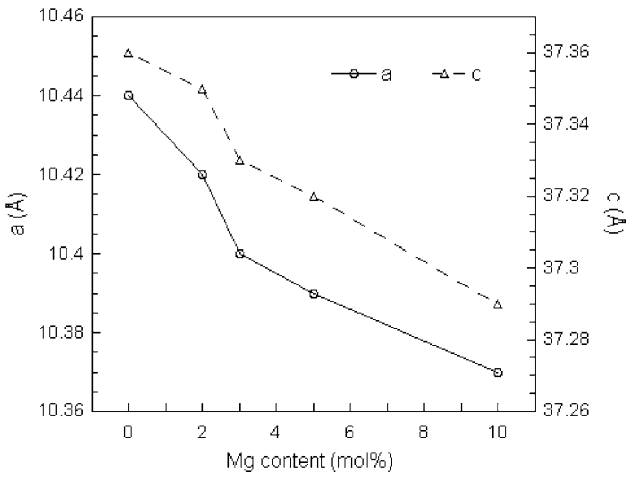

Fig. 4 Influence of incorporation of Mg^{2+} in β-TCP structure on the lattice parameters 'a' and 'c'

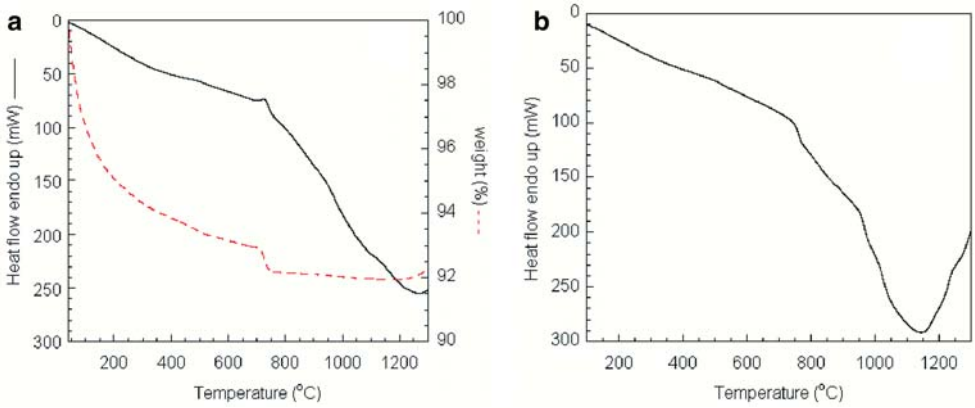

Fig. 5 TG/DTA results of β-TCMP-3 precursor (**a**) and DTA curve of β-TCP powder (**b**) heated in air up to 1,300°C

β-TCP powder heated in air at a heating rate of 5°C/min to 1,000°C and 2°C/min from 1,000 to 1,300°C. The exothermic peak around 1,150°C indicates the phase transformation from β-TCP to α-TCP.

Figure 6 shows XRD pattern of β-TCP and β-TCMP samples after calcination at different temperatures. Diffraction peak (034) from α-TCP (JCPDF #29-0359) was found in β-TCP sample after being calcined at 1,150°C (Fig. 6a), which is consistent with the DTA result (Fig. 5b). α-TCP was also found in β-TCMP-2 after being calcined at 1,250°C (Fig. 6b). No peak from α-TCP was found in β-TCMP-3 and β-TCMP-4 after calcination at 1,300°C for 2 h, indicating that the phase transition temperature from β-TCP to α-TCP in these samples exceeds 1,300°C. These results demonstrate that the transition temperature from β-TCP to α-TCP increases with the increase of Mg content in β-TCMP [13].

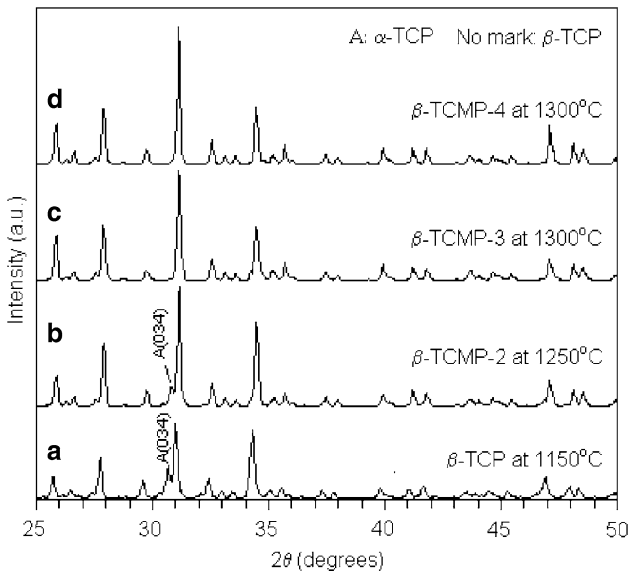

Fig. 6 XRD pattern of β-TCP and β-TCMP samples after calcination at different temperatures for 2 h: (**a**) pure β-TCP at 1,150°C, (**b**) β-TCMP-2 at 1,250°C, (**c**) β-TCMP-3 and (**d**) β-TCMP-4 at 1,300°C

3.2 Ceramic density and microstructures

Figure 7 shows density of β-TCP and β-TCMP-3 ceramics measured by Archimedes' method with deionized water. For each ceramic, 10–15 samples were used and the results averaged. For β-TCP ceramics, the average density of ceramics sintered at 1,150°C and 1,250°C are lower than that of ceramics sintered at 1,100°C. This is caused by the formation of α-TCP in the ceramics sintered at 1,150°C and 1,250°C, which is indicated by the bulk XRD pattern (Fig. 8b and c) of the ceramics. β-TCP ($a = b = 10.44$ Å, $c = 37.38$ Å, $\alpha = \beta = 90°$, $\gamma = 120°$, cell volume = 3,513 Å^3) to α-TCP ($a = 12.89$ Å, $b = 27.28$ Å, $c = 15.22$ Å, $\alpha = \gamma = 90°$, $\beta = 126.2°$, cell volume = 4,318 Å^3) [24] transformation causes the expansion of TCP during the sintering process, which prevents the TCP ceramics from further densification.

For β-TCMP-3 ceramics, only the β-TCP phase exists when sintered below 1,300°C (Fig. 6c). Ceramic density

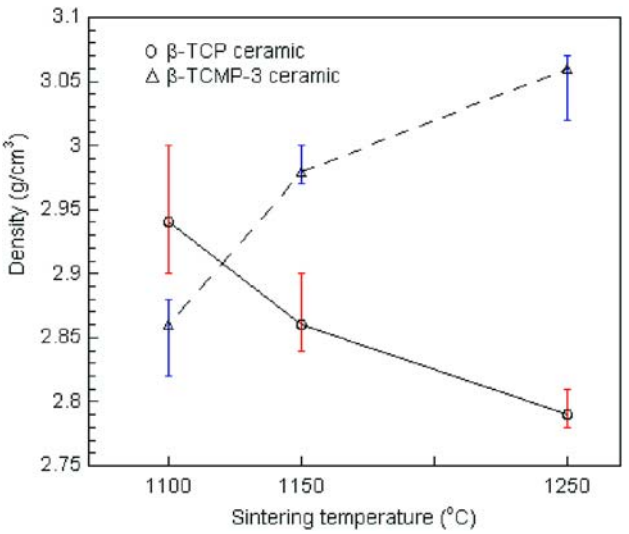

Fig. 7 Average density of β-TCP and β-TCMP-3 ceramics sintered at different temperatures for 2 h with error bars

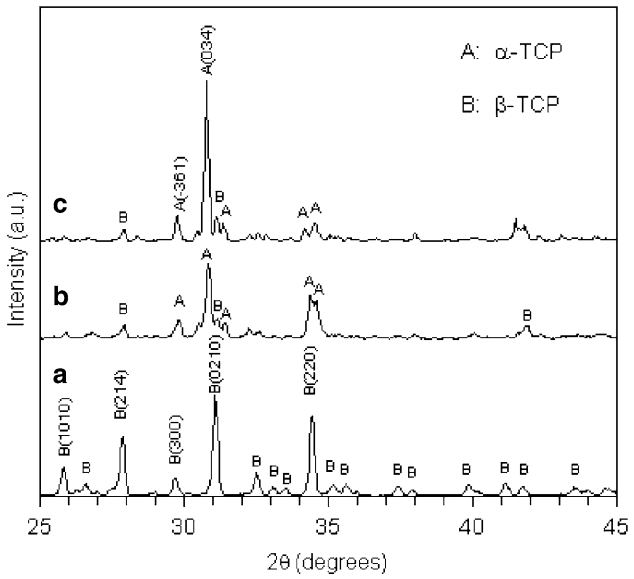

Fig. 8 Bulk XRD pattern of β-TCP ceramics sintered at different temperatures: (**a**) 1,100°C, (**b**) 1,150°C and (**c**) 1,250°C

increases with increasing sintering temperature (Fig. 7). The theoretical density of β-TCMP-3 is calculated to be 3.08 g cm^{-3}, based on the refined lattice constants ($a = b = 10.40$ Å, $c = 37.33$ Å, $\alpha = \beta = 90°$, $\gamma = 120°$) from the XRD patterns. β-TCMP-3 ceramics sintered at 1,150°C and 1,250°C, have average density of 2.98 g cm^{-3} and 3.06 g cm^{-3}, with relative density of 96.8% and 99.4%, respectively. These results indicate that extremely dense β-TCMP ceramics can be prepared by sintering the ceramics above 1,150°C without the formation of α-TCP.

SEM images of surfaces of β-TCP ceramics sintered at different temperatures are shown in Fig. 9. β-TCP ceramics sintered at 1,100°C (Fig. 9a) had a grain size of several micrometers. A small amount of voids were found around grains, and were nearly micro-crack free. After being sintered at 1,150°C (Fig. 9b), larger cracks were observed in the ceramics, and some micro-cracks generated from the main cracks were also detected. The transformation from β-TCP to α-TCP can be observed by the formation of new continuous phase (α-TCP) around the original β-TCP particles, which is consistent with the XRD result (Fig. 8b). The formation of α-TCP caused the expansion of ceramics, decreased the density (Fig. 7) and created cracks.

After sintered at 1,250°C, ceramics are mainly composed of α-TCP, which is indicated by the XRD result (Fig. 8c). New grain boundaries of α-TCP can be observed, and the grain size is about several micrometers (Fig. 9c and d). More cracks were found in the ceramics (Fig. 9c), compared to ceramics sintered at 1,150°C. Micro-cracks (marked with arrows) were found even in dense portions of the sample (Fig. 9d). Both intergranular and transgranular cracks are found in the ceramic samples sintered at 1,150°C and 1,250°C.

Figure 10 shows SEM images of surfaces of β-TCMP-3 ceramics sintered at different temperatures. Voids around grains were found as the main defects in the ceramics sintered at 1,100°C (Fig. 10a). Compared with β-TCP ceramics (Fig. 9a), a larger amount of voids were found in β-TCMP-3 samples. The grain size is about 1–4 μm (Fig. 10a). Without any apparent phase transformation, β-TCMP grains grew up to 10 μm when sintered at 1,150°C (Fig. 10b), and up to 20 μm at 1,250°C (Fig. 10c).

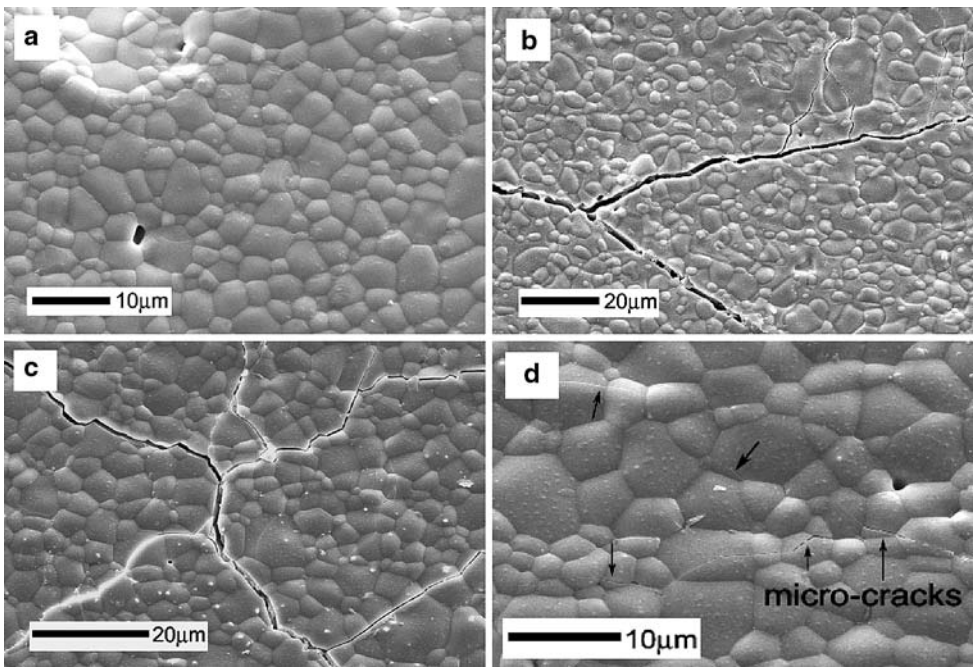

Fig. 9 SEM images of surfaces of β-TCP ceramics sintered at different temperatures: (**a**) 1,100°C, (**b**) 1,150°C, (**c**) and (**d**) 1,250°C

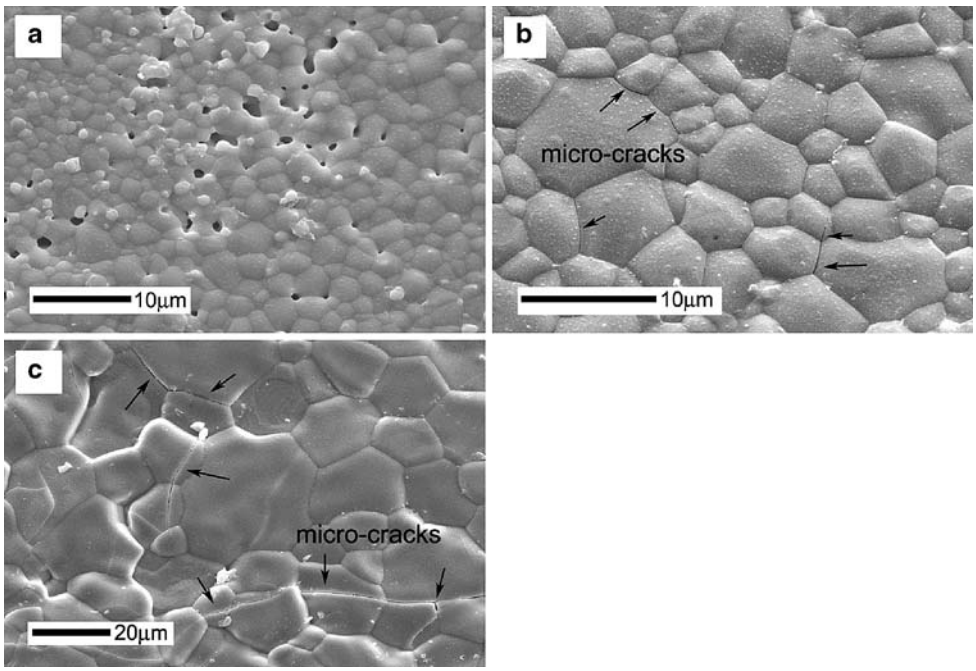

Fig. 10 SEM images of surfaces of β-TCMP-3 ceramics sintered at different temperatures: (**a**) 1,100°C, (**b**) 1,150°C, and (**c**) 1,250°C

As a result of grain growth with the increase of sintering temperature, the apparent density of β-TCMP-3 ceramics also increased, as denoted by the absence of significant voids, which is consistent with density measurement (Fig. 7). Both intergranular and transgranular micro-cracks were found in β-TCMP-3 ceramics sintered above 1,150°C (Fig. 10b and c), which may be caused by contraction of the ceramics during the sintering process.

3.3 Mechanical strength of the CaP ceramics

Figure 11 shows typical stress-stain curves of β-TCP and β-TCMP-3 ceramics. The curves show a failure model of brittle materials. There are uncertainties in performing mechanical tests of ceramics in this investigation, due to the difference in specimen dimensions, existence of voids (Figs. 9a and 10a), macro-cracks (Fig. 9b and c) or micro-cracks (Fig. 10b and c). The compressive strength of ceramics varies from specimen to specimen, which is indicated by Weibull distribution (Fig. 12) of fracture stress of β-TCP and β-TCMP-3 ceramics sintered at 1,100°C. Weibull analysis is applied by means of the following equation [26–28]:

$$P(V) = \exp\left[-\left(\frac{\sigma}{\sigma_0}\right)^m\right] \quad (5)$$

where P(V) is the survival probability, σ_0 and m are Weibull parameters obtained experimentally, and σ is the compressive strength. The Weibull parameter 'm' for β-TCP and β-TCMP-3 ceramics is 5.92 and 4.22, respectively. The plots indicate that the 50% fracture probabilities ($P(V) = 0.5$) of

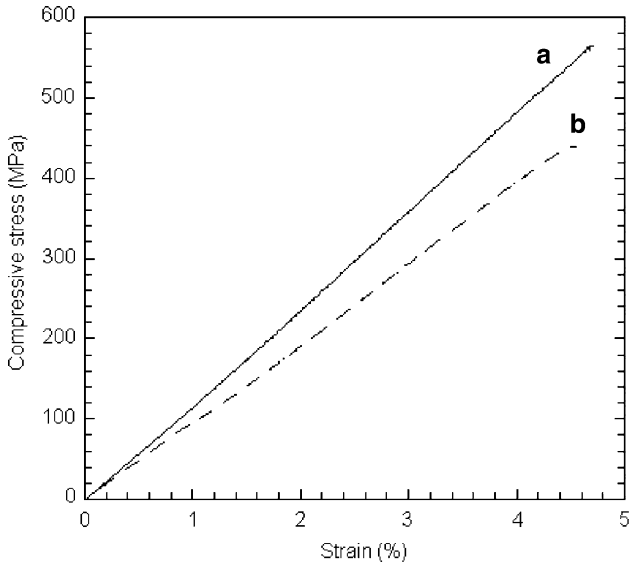

Fig. 11 Quasi-static compressive stress–strain curves of (**a**) β-TCP and (**b**) β-TCMP-3 ceramics sintered at 1,100°C for 2 h

β-TCP and β-TCMP-3 ceramics are ~540 MPa and 440 MPa, respectively, which are close to the average fracture strength of these two ceramics, 540 MPa and 430 MPa.

The average compressive strength of β-TCP and β-TCMP-3 ceramics are shown in Fig. 13. The average strength of β-TCP ceramics sintered at 1,100°C is ~540 MPa. These ceramics are pure β-TCP, indicating by the XRD result (Fig. 8a), and micro-voids are the main defects (Fig. 9a). Most ceramics sintered at 1,100°C

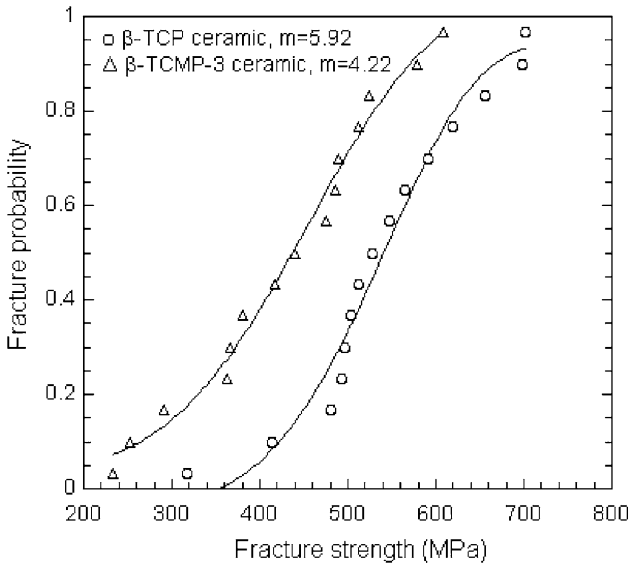

Fig. 12 Weibull distribution of fracture stress of β-TCP and β-TCMP-3 ceramics sintered at 1,100°C for 2 h

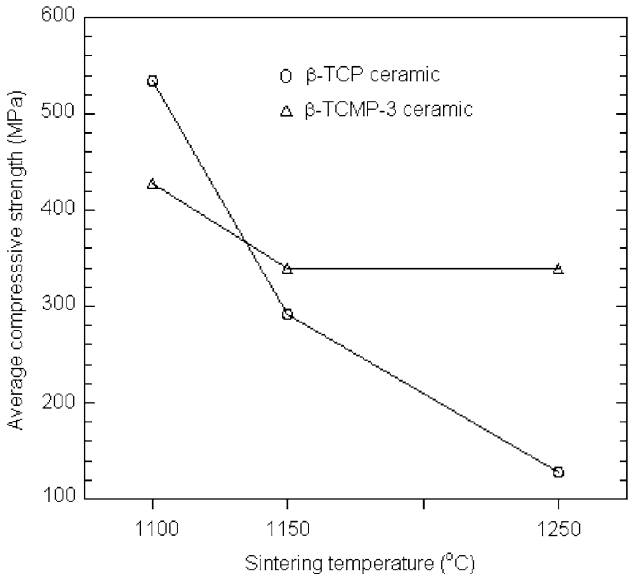

Fig. 13 Average compressive strength of β-TCP and β-TCMP-3 ceramics sintered at different temperatures for 2 h

fractured into small particles after failure in the compression tests. Ceramics sintered at 1,150°C and 1,250°C have an average strength ~290 MPa and 130 MPa, respectively. These ceramics have α-TCP as the main phase (Fig. 8b and c) and macro- or micro-cracks as the main defects (Fig. 9b–d). After failure in the compression tests, larger particles or pieces formed from these ceramics, consistent with pre-existing cracks in the samples. The above results demonstrate that the formation of α-TCP at temperatures above 1,150°C, create cracks in the ceramics and decreased the mechanical strength.

The average compressive strength of β-TCMP-3 ceramics sintered at 1,100°C is ~430 MPa, slightly lower than that of β-TCP ceramics (540 MPa), due to a larger amount of micro-voids in the β-TCMP-3 ceramics (Fig. 10a) compared with the β-TCP ceramics (Fig. 9a). β-TCMP-3 ceramics sintered at 1,150°C and 1,250°C have the same average strength of ~340 MPa, which is lower than that of β-TCMP-3 ceramics sintered at 1,100°C. Although the density of β-TCMP-3 ceramics increased with the increase of sintering temperature (Fig. 7), the existence of micro-cracks and grain growth in the ceramics (Fig. 10b and c) sintered at temperatures above 1,150°C decreased the mechanical strength.

4 Conclusions

β-TCP or β-TCMP powders can be prepared by a two-step process: wet precipitation of apatitic tricalcium phosphate ('precursor') and calcination of the precursor at 800°C for 3 h. With the increasing Mg^{2+} content in the β-TCP structure, the transition temperature from β-TCP to α-TCP increases. β-TCMP-3 (3 mol.% Mg^{2+}) has a transition temperature above 1,300°C.

β-TCP ceramics prepared by pressing the green body at 100 MPa and sintering at 1,100°C, have high average strength of 540 MPa. β-TCP ceramics sintered above 1,150°C have α-TCP as the main phase, which caused the expansion of ceramics, decreased the ceramic density and created cracks in the samples. These pre-existing cracks in the ceramics caused fracture along the cracks and decreased the compressive strength of the ceramics.

Dense β-TCMP-3 ceramics were prepared by sintering at temperature above 1,150°C. The average relative density of β-TCMP-3 ceramics sintered at 1,150°C and 1,250°C are 96.8% and 99.4%, respectively. However, the formation of micro-cracks and grain growth in dense β-TCMP-3 ceramics sintered above 1,150°C decreased the compressive strength of the ceramics.

References

1. F. Peters, D. Reif, Mat-wiss u Werkstofftech **35**, 203 (2004)
2. N. Kondo, A. Ogose, K. Tokunaga, T. Ito, K. Arai, N. Kudo, H. Inoue, H. Irie, N. Endo, Biomaterials **26**, 5600 (2005)
3. H.E. Koepp, S. Schorlemmer, S. Kessler, R.E. Brenner, L. Claes, K.P. Günther, A.A. Ignatius, J. Biomed. Mater. Res. Part B Appl. Biomater. **70**, 209 (2004)
4. N. Matsushita, H. Terai, T. Okada, K. Nozaki, H. Inoue, S. Miyamoto, K. Takaoka, J. Biomed. Mater. Res. Part A **70**, 450 (2004)
5. P. Miranda, E. Saiz, K. Gryn, A.P. Tomsia, Acta Biomater. **2**, 457 (2006)
6. P.N. Kumta, C. Sfeir, D.H. Lee, D. Olton, D. Choi, Acta Biomater. **1**, 65 (2005)
7. R. Famery, N. Richard, P. Boch, Ceram. Int. **20**, 327 (1994)

8. M. Descamps, J.C. Hornez, A. Leriche, J. Eur. Ceram. Soc. **27**, 2401 (2007)
9. M. Yashima, A. Sakai, Chem. Phys. Lett. **372**, 779 (2003)
10. K. Itatani, M. Takahashi, F.S. Howell, M. Aizawa, J. Mater. Sci. Mater. Med. **13**, 707 (2002)
11. A. Tampieri, G. Celotti, F. Szontagh, E. Landi, J. Mater. Sci. Mater. Med. **8**, 29–37 (1997)
12. K. Itatani, T. Nishioka, S. Seike, F.S. Howell, A. Kishioka, M. Kinoshita, J. Am. Ceram. Soc. **77**, 801 (1994)
13. R. Enderle, F. Götz-Neunhoeffer, M. Göbbels, F.A. Müller, P. Greil, Biomaterials **26**, 3379 (2005)
14. D.M.B. Wolff, E.G. Ramalho, W. Acchar, Mater. Sci. Forum **530–531**, 581 (2006)
15. J. Marchi, A.C.S. Dantas, P. Greil, J.C. Bressiani, A.H.A. Bressiani, F.A. Müller, Mater. Res. Bull. **42**, 1040 (2007)
16. K.D. Groot, *Bioceramics of Calcium Phosphate* (CRC Press, Boca Raton, Florida, 1983)
17. R. Lagier, C.A. Baud, Pathol. Res. Pract. **199**, 329 (2003)
18. L.M. Ryan, H.S. Cheung, R.Z. LeGeros, I.V. Kurup, J. Toth, P.R. Westfall, G.M. McCarthy, Calcif. Tissue Int. **65**, 374 (1999)
19. K.S. Vecchio, X. Zhang, J.B. Massie, M. Wang, C.W. Kim, Acta Biomater. **3**, 785 (2007)
20. A. Destainville, E. Champion, D. Bernache-Assollant, E. Laborde, Mater. Chem. Phys. **80**, 269 (2003)
21. J.J. Prieto Valdés, J. Ortiz López, G. Rueda Morales, G. Pacheco Malagon, V. Prieto Gortcheva, J. Mater. Sci. Mater. Med. **8**, 297 (1997)
22. I.R. Gibson, I. Rehman, S.M. Best, W. Bonfield, J. Mater. Sci. Mater. Med. **12**, 799 (2000)
23. S. Kannan, A.F. Lemos, J.H.G. Rocha, J.M.F. Ferreira, J. Am. Ceram. Soc. **89**, 2757 (2006)
24. J.C. Elliott, *Structure and Chemistry of the Apatites and Other Calcium Orthophosphates* (Elsevier Science, Amsterdam, The Netherlands, 1994)
25. C. Tardei, F. Grigore, I. Pasuk, S. Stoleriu, J. Optoelectron. Adv. Mater. (JOAM) **8**, 568 (2006)
26. J.B. Wachtman, *Mechanical Properties of Ceramics* (Wiley-Interscience, New York, 1996)
27. R. Menig, M.H. Meyers, M.A. Meyers, K.S. Vecchio, Mater. Sci. Eng. A **297**, 203 (2001)
28. R. Menig, M.H. Meyers, M.A. Meyers, K.S. Vecchio, Acta Mater. **48**, 2383 (2000)